IL NUOVO CIMENTO Vol. 24 C, N. 2 Marzo-Aprile 2001

Chaos and weather prediction - A review of recent advances in Numerical Weather Prediction: Ensemble forecasting and adaptive observation targeting

R. Buizza(*)

European Centre for Medium-Range Weather Forecasts
Shinfield Park, Reading, Berkshire, RG2 9AX, UK

(ricevuto l'8 Maggio 2000; revisionato il 10 Dicembre 2000; approvato il 23 Gennaio 2001)

Summary. — The weather is a chaotic system. Small errors in the initial conditions of a forecast grow rapidly and predictability is limited by model errors due to the approximate simulation of atmospheric processes of the state-of-the-art numerical models. These two sources of uncertainties limit the skill of single, deterministic forecasts in an unpredictable way, with days of high/poor quality forecasts randomly followed by days of high/poor quality forecasts. Two recent advances in numerical weather prediction, the operational implementation of ensemble prediction systems and the development of objective procedures to target adaptive observations are discussed. These advances have been thought and designed to reduce forecast errors and to provide forecasters with more complete weather predictions. Ensemble prediction is a feasible method to estimate the probability distribution function of forecast states. Ensemble systems can provide forecasters with an objective way to predict the skill of single deterministic forecasts. Adaptive observations targeted in sensitive regions can reduce the initial conditions' uncertainties, and thus decrease forecast errors. Singular vectors that identify unstable regions of the atmospheric flow can be used to identify optimal ways to adapt the atmospheric observing system. The European Centre for Medium-Range Weather Forecasts Ensemble Prediction System is described, and targeting experiments are discussed.

PACS 92.60.−e – Meteorology.
PACS 92.60.Wc – Weather analysis and prediction.
PACS 47.52.+j – Chaos.

1. – Introduction

A dynamical system shows a chaotic behavior if most orbits exhibit sensitive dependence (Lorenz, 1993). An orbit is characterized by sensitive dependence if most other

(*) E-mail: buizza@ecmwf.int

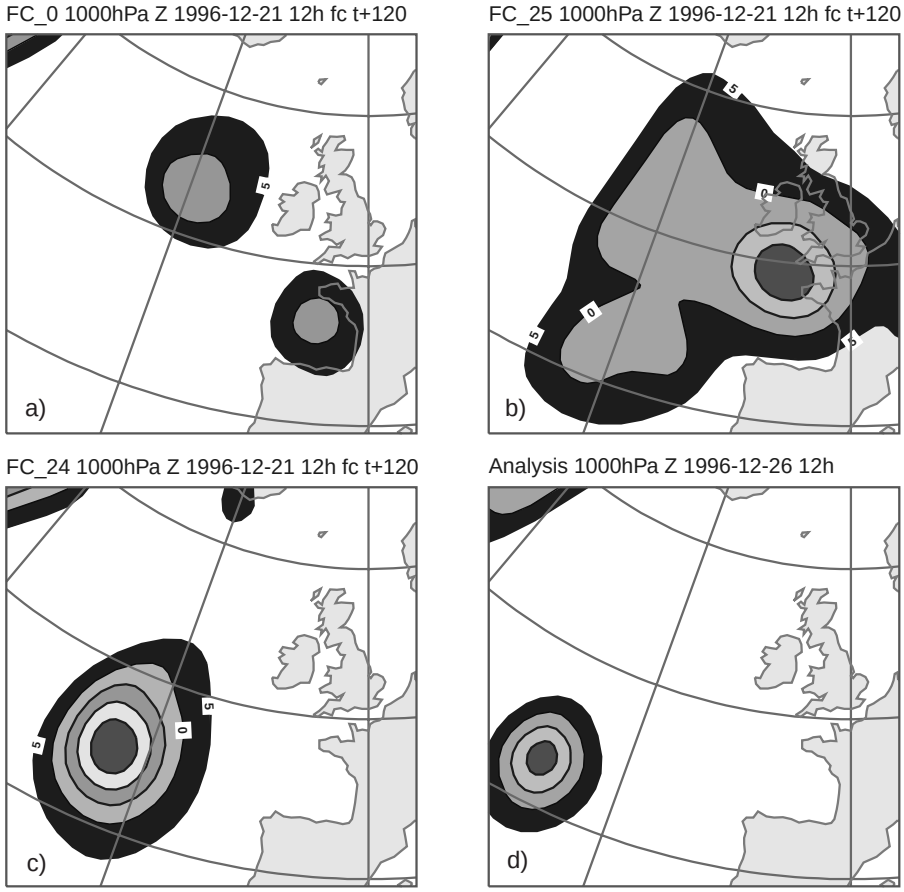

Fig. 1. – (a–c) Forecast for the geopotential height at 1000 hPa (this field illustrates the atmospheric state close to the surface) given by three forecasts started from very similar initial conditions, and (d) verifying analysis. Contour interval is 5 m, with only values smaller than 5 m shown.

orbits that pass close to it at some point do not remain close to it as time advances.

The atmosphere exhibits this behavior. Figure 1 shows three different weather forecasts, all started from very similar initial conditions. The differences among the three initial conditions were smaller than estimated analysis errors, and each of the three initial conditions could be considered as an equally probable estimate of the "true" initial state of the atmosphere. After 5 days of numerical integration, the three forecasts evolved into very different atmospheric situations. In particular, note the different positions of the cyclone forecast in the Eastern Atlantic approaching United Kingdom (fig. 1(a–c)). The first forecast indicated two areas of weak cyclonic circulation west and south of the British Isles; the second forecast positioned a more intense cyclone southwest of Cornwall, and the third forecast kept the cyclone in the open seas. This latter turned out to be the most accurate when compared to the observed atmospheric state (fig. 1(d)).

The atmosphere is an intricate dynamical system with many degrees of freedom. The state of the atmosphere is described by the spatial distribution of wind, temperature, and other weather variables (*e.g.*, specific humidity and surface pressure). The mathe-

matical differential equations describing the system time evolution include Newton's laws of motion used in the form "acceleration equals force divided by mass" and the laws of thermodynamics.

Richardson (1922) can be considered the first to have shown that the weather could be predicted numerically. In his work, he approximated the differential equations governing the atmospheric motions with a set of algebraic difference equations for the tendencies of various field variables at a finite number of grid points in space. By extrapolating the computed tendencies ahead in time, he could predict the field variables in the future. Unfortunately, his results were very poor, both because of deficient initial data, and because of serious problems in his approach.

After World War II the interest in numerical weather prediction revived, partly because of an expansion of the meteorological observation network, but also because of the development of digital computers. Charney (1947, 1948) developed a model applying an essential filtering approximation of the Richardson's equations, based on the so-called geostrophic and hydrostatic equations. In 1950, an electronic computer (ENIAC) was installed at Princeton University, and Charney, Fjørtoft and Von Neumann and Ritchmeyer (1950) made the first numerical prediction using the equivalent barotropic version of Charney's model. This model provided forecasts of the geopotential height near 500 hPa, and could be used as an aid to provide explicit predictions of other variables as surface pressure and temperature distributions. Charney's results led to the developments of more complex models of the atmospheric circulation, the so-called global circulation models.

With the introduction of powerful computers in meteorology, the meteorological community invested more time and efforts to develop more complex numerical models of the atmosphere. One of the most complex models used routinely for operational weather prediction is the one implemented at the European Centre for Medium-Range Weather Forecasts (ECMWF). At the time of writing (December 2000), the ECMWF model (Simmons *et al.*, 1989, Courtier *et al.*, 1991, Simmons *et al.*, 1995) is integrated with a horizontal spectral triangular truncation T_L511 (the subscript L indicates that a linear grid is used in grid-point space) and with 60 vertical levels. The model includes a parameterization of many physical processes such as surface and boundary layer processes (Viterbo and Beljaars, 1995) radiation (Mocrette, 1990) and moist processes (Tiedtke, 1993, Jacob, 1994).

The initial conditions of any numerical integration is given by a very complex assimilation procedure that estimates the state of the atmosphere by considering all available observations. This computational process is referred to as data assimilation (Talagrand and Courtier, 1987, Courtier and Talagrand, 1987, Courtier *et al.*, 1994). The fact that a limited number of observations are available (limited compared to the degrees of freedom of the system) and that part of the globe is characterized by a very poor coverage introduces uncertainties in the initial conditions. The presence of uncertainties in the initial conditions is the first source of forecast errors.

A requirement for skilful predictions is that numerical models are able to accurately simulate the dominant atmospheric phenomena. The fact that the description of some physical processes has only a certain degree of accuracy, and the fact that numerical models simulate only processes with certain spatial and temporal, is the second source of forecast errors. Computer resources contribute to limit the complexity and the resolution of numerical models and assimilation, since, to be useful, numerical predictions must be produced in a reasonable amount of time.

These two sources of forecast errors cause weather forecasts to deteriorate with forecast time.

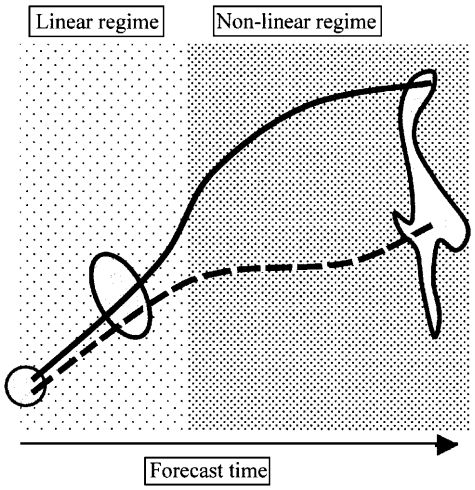

Fig. 2. – The deterministic approach to numerical weather prediction provides one single forecast (continuous line) for the "true" time evolution of the system (dashed line). The ensemble approach to numerical weather prediction tries to estimate the probability density function of forecast states (white shapes). Ideally, the ensemble probability density function estimate includes the true state of the system as a possible solution.

Initial conditions will always be known approximately, since each data is characterized by an error that depends on the instrumental accuracy. Observational errors, usually in the smaller scales, amplify and through non-linear interactions spread to longer scales, eventually affecting the skill of these latter ones (Somerville, 1979).

The error growth of the 10-day forecast of the ECMWF model from 1 December 1980 to 31 May 1994 was analyzed in great detail by Simmons *et al.* (1995). It was concluded that 15 years of research had improved substantially the accuracy over the first half of the forecast range (say up to forecast day 5), but that there had been little error reduction in the late forecast range. While this applied on average, it was also pointed out that there had been improvements in the skill of the good forecasts. In other words, good forecasts had higher skill in the nineties than before. The problem was that it was difficult to assess *a priori* whether a forecast would be skilful or unskillful using only a deterministic approach to weather prediction.

A complete description of the weather prediction problem can be stated in terms of the time evolution of an appropriate probability density function (PDF) in the atmosphere's phase space (fig. 2). Although this problem can be formulated exactly through the continuity equation for probability (Liouville equation, see, *e.g.*, Ehrendorfer, 1994), ensemble prediction based on a finite number of deterministic integrations appears to be the only feasible method to predict the PDF beyond the range of linear error growth.

Since December 1992, both the U. S. National Center for Environmental Predictions (NCEP, previously NMC) and ECMWF have integrated their deterministic high-resolution prediction with medium-range ensemble prediction (Tracton and Kalnay, 1993, Palmer *et al.*, 1993). These developments followed the theoretical and experimental work of, among others, Epstein (1969), Gleeson (1970), Fleming (1971a-b) and Leith (1974).

NCEP and ECMWF followed the same strategy of providing an ensemble of forecasts computed with the same model, one started with unperturbed initial conditions

referred to as the "control" forecast and the others with initial conditions defined adding small perturbations to the control initial condition. Broadly speaking, the two ensemble systems differ in the ensemble size, in the fact that at NCEP a combination of lagged forecasts is used, and in the definition of the perturbed initial. The reader is referred to Toth and Kalnay (1993) for the description of the "breeding" method applied at NMC and to Buizza and Palmer (1995) for a thorough discussion of the singular vector approach followed at ECMWF.

A different methodology was followed few years later at the Atmospheric Environment Service (AES, Canada), where a system simulation approach was used to generate an ensemble of initial perturbations (Houtekamer *et al.*, 1996). At AES, a number of parallel data assimilation cycles is run randomly perturbing the observations, and using different parameterisation schemes for some physical processes in each run. The ensemble of initial states generated by the different data assimilation cycles defines the initial conditions of the Canadian ensemble system. Moreover, forecasts started from such an ensemble of initial conditions are used to estimate forecast-error statistics (Evensen, 1994, Houtekamer and Mitchell, 1998).

Ensemble prediction can be considered one of the most recent advances in numerical weather prediction: it is the first topic discussed in this work. The development of objective procedures to target adaptive observations is the second topic.

The idea of targeting adaptive observations is based on the fact that weather forecasting can be improved by adding extra observations only in sensitive regions. These sensitive regions can be identified using tangent forward and adjoint versions of numerical weather prediction models (Thorpe *et al.*, 1998, Buizza and Montani, 1999). Instruments can be deployed in the identified sensitive regions to take the required observations using pilot-less aircraft, or energy-intensive satellite instruments can be activated to sample the sensitive regions with higher frequency.

After this Introduction, sect. **2** describes some early results by Lorenz, and illustrates the chaotic behavior of a simple 3-dimension system. In sect. **3** the main steps of numerical weather prediction are delineated. The impact of initial condition and model uncertainties on numerical integration is discussed in sect. **4**. The ECMWF Ensemble Prediction System is described in sect. **5**. Targeting adaptive observations using singular vectors is discussed in sect. **6**. Conclusions are reported in sect. **7**. Mathematical details are reported in two appendices.

2. – The Lorenz system

One of the fathers of chaos theory is E. Lorenz (1963, 1965, 1993). Results from the 3-dimentional Lorenz system

$$\begin{aligned} \dot{X} &= -\sigma X + \sigma Y, \\ \dot{Y} &= -XZ + rX - Y, \\ \dot{Z} &= XY - bZ, \end{aligned} \tag{1}$$

illustrate the dispersion of finite time integrations from an ensemble of initial conditions (fig. 3). the different initial points can be considered as estimates of the "true" state of the system (which can be thought of as any point inside ellipsoid), and the time evolution of each of them as possible forecasts. Subject to the initial "true" state of the system,

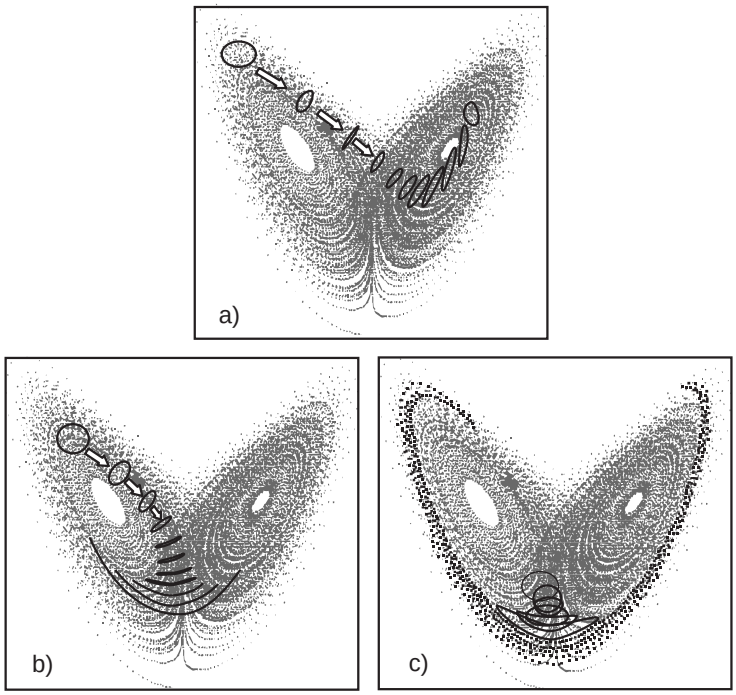

Fig. 3. – Lorenz attractor with superimposed finite-time ensemble integration.

points close together at initial time diverge in time at different rates. Thus, depending on the point chosen to describe the system time evolution, different forecasts are obtained.

The two wings of the Lorenz attractor can be considered as identifying two different weather regimes, for example one warm and wet and the other cold and sunny. Suppose that the main purpose of the forecast is to predict whether the system is going through a regime transition. When the system is in a predictable initial state (fig. 3a), the rate of forecast diverge is small, and all the points stay close together till the final time. Whatever the point chosen to represent the initial state of the system, the forecast is characterised by a small error, and a correct indication of a regime transition is given. The ensemble of points can be used to generate probabilistic forecasts of regime transitions. In this case, since all points end in the other wing of the attractor, there is a 100% probability of regime transition.

By contrast, when the system is in a less predictable state (fig. 3b), the points stay close together only for a short time period, and then start diverging. While it is still possible to predict with a good degree of accuracy the future forecast state of the system for a short time period, it is difficult to predict whether the system will go through a regime transition in the long forecast range. Figure 3c shows an even worse scenario, with points diverging even after a short time period, and ending in very distant part of the system attractor. In probabilistic terms, one could have only predicted that there is a 50% chance of the system undergoing a regime transition. Moreover, the ensemble of points indicates that there is a greater uncertainty in predicting the region of the system attractor where the system will be at final time in the third case (fig. 3c).

The comparison of the points' divergence during the three cases indicates how en-

semble prediction systems can be used to "forecast the forecast skill". In the case of the Lorenz system, a small divergence is associated to a predictable case, and confidence can be attached to any of the single deterministic forecasts given by the single points. By contrast, a large diverge indicate low predictability.

Similar sensitivity to the initial state is shown in weather prediction. Figure 4 shows the forecasts for air temperature in London given by 33 different forecasts started from very similar initial conditions for two different dates, 26 June 1995 and 26 June 1994. There is a clear different degree of divergence during the two cases. All forecasts stay close together up to forecast day 10 for the first case (fig. 4(a)), while they all diverge already at forecast day 3 in the second case (fig. 4(b)). The level of spread among the different forecasts can be used as a measure of the predictability of the two atmospheric states.

3. – Numerical weather prediction

Numerical weather prediction is realised by integrating primitive-equation models. The equations are solved by replacing time derivatives by finite differences, and spatially either by finite difference schemes or spectral methods. The state of the atmosphere is described at a series of grid-points by a set of state variables such as temperature, velocity, humidity and pressure.

At the time of writing (December 2000) the ECMWF high-resolution deterministic model is integrated with a spectral triangular truncation T_L511, which is equivalent to a grid-point spacing of about 40 km, and 60 vertical levels.

Meteorological observations made all over the world (fig. 5) are used to compute the best estimate of the system initial conditions. Some of these observations, such as the ones from weather balloons or radiosondes, are taken at specific times at fixed locations (fig. 6). Other data, such as the ones from aircrafts, ships or satellites, are not fixed in space. There is a great variability in the observation network, with data over land/oceanic regions characterised by very high/coarse density.

Observations cannot be used directly to start model integration, but must be modified in a dynamically consistent way to obtain a suitable data set. This process is usually referred to as data assimilation. At the time of writing (December 2000), ECMWF uses a 4-dimensional data assimilation scheme to estimate the actual state of the atmosphere (Courtier *et al.*, 1994).

In the ECMWF model, dynamical quantities as pressure and velocity gradients are evaluated in spectral space, while computations involving processes such as radiation, moisture conversion, turbulence, are calculated in grid-point space. This combination preserves the local nature of physical processes, and retains the superior accuracy of the spectral method for dynamical computation.

The physical processes associated with radiative transfer, turbulent mixing, moist processes, are active at scales smaller than the horizontal grid size. The approximation of unresolved processes in terms of model-resolved variables is referred to as parameterisation (fig. 7). The parameterisation of physical processes is probably one of the most difficult and controversial area of weather modelling (Holton, 1992).

4. – Sources of forecast error

Indications of the relative importance of the initial and model uncertainties on forecast error can be deduced from the works of Downton and Bell (1988) and Richardson (1998),

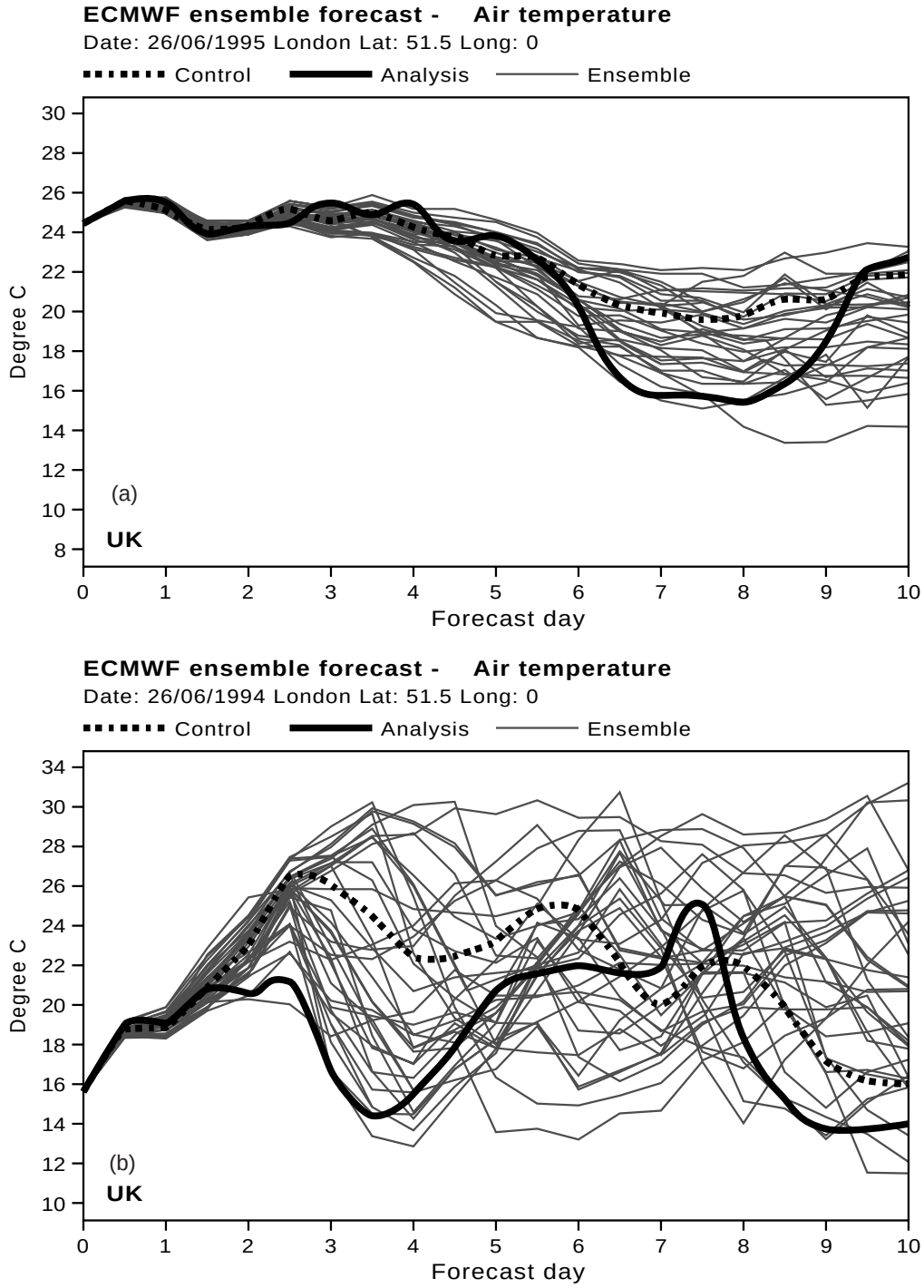

Fig. 4. – ECMWF forecasts for air temperature in London started from (a) 26 June 1995 and (b) 26 June 1994.

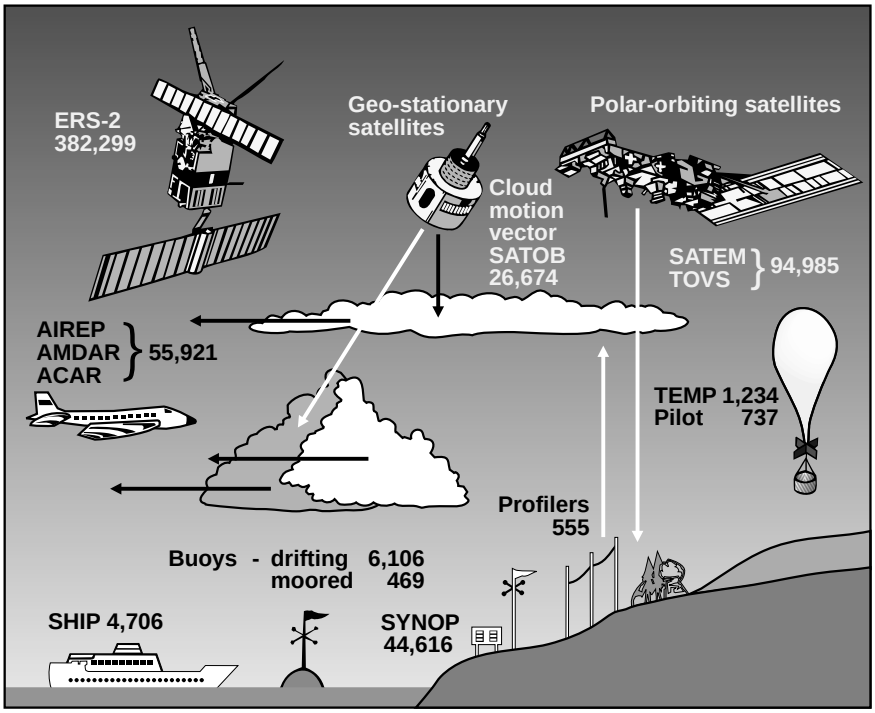

Fig. 5. – Type and number of observations used to estimate the atmosphere initial conditions in a typical day.

who compared forecasts given by the UKMO (United Kingdom Meteorological Office) and the ECMWF forecasting systems. In these studies, substantial forecast differences

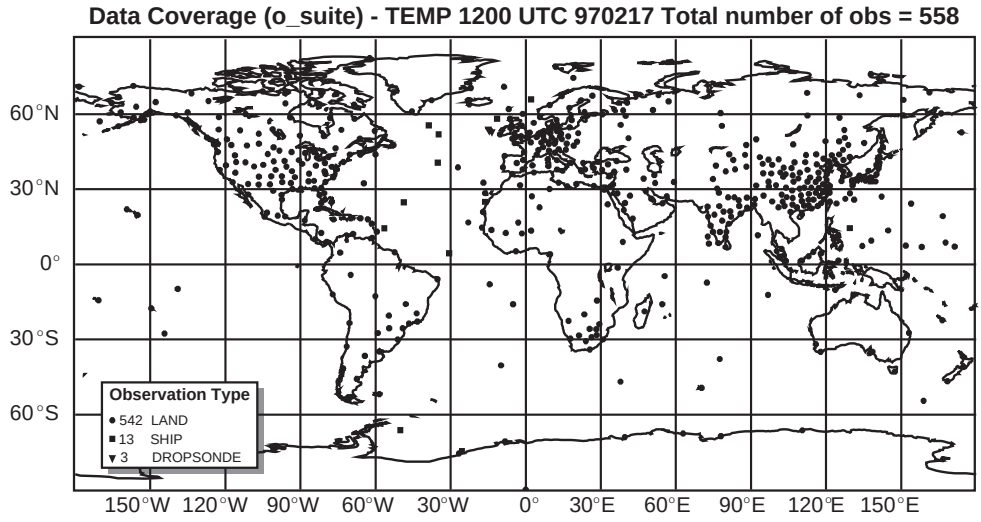

Fig. 6. – Map of radiosonde locations.

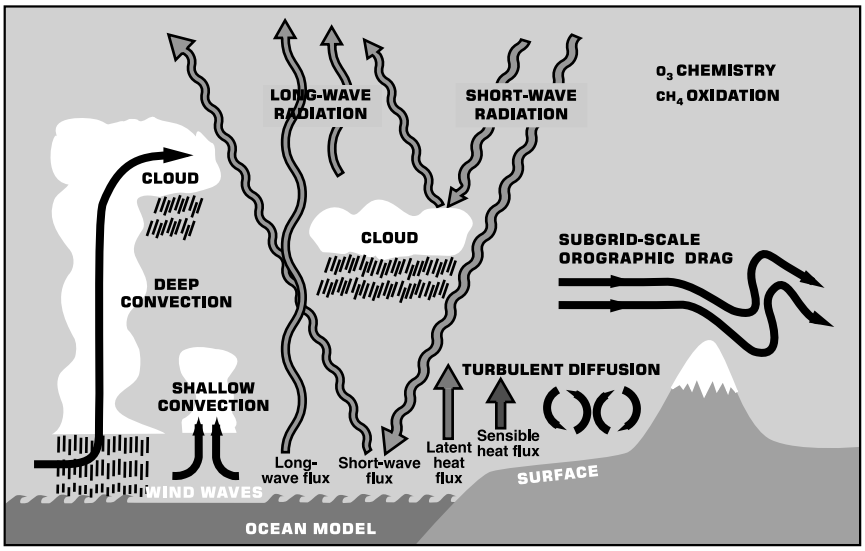

Fig. 7. – Schematic diagram of the different physical processes represented in the ECMWF model.

between the ECMWF and the UKMO operational forecasts could mostly be traced to differences between the two operational analyses, rather than between the two forecast models. On the other hand, recent results from Harrison *et al.* (1999) indicate that the impact of model uncertainties on forecast error cannot be ignored.

These results suggest that an ensemble system should certainly simulate the presence of uncertainties in the initial conditions, since this is the dominant effect, but it should also simulate model uncertainties.

The first version of the ECMWF Ensemble Prediction System (hereafter EPS, Palmer *et al.*, 1993, Molteni *et al.*, 1996) implemented operationally in December 1992 included only a simulation of initial uncertainties. A similar "perfect model" strategy was followed at the US National Centers for Environmental Prediction (NCEP, Tracton and Kalnay, 1993).

Houtekamer *et al.* (1996) first included model uncertainties in the ensemble prediction system developed at the Atmospheric Environment Service in Canada. Following a system simulation approach to ensemble prediction, they developed a procedure where each ensemble member differs both in the initial conditions, and in sub-grid scale parameters. In this approach, each ensemble member is integrated using different parameterizations of horizontal diffusion, convection, radiation, gravity wave drag, and with different orography.

There are certainly good grounds for believing that there is a significant source of random error associated with the parameterized physical processes. For example, consider a grid point over the tropical warm pool area during a period of organized deep convection. By definition, the actual contributions to the tendencies due to parameterized physical processes are often associated with organized mesoscale convective systems whose spatial extent may be comparable with the model resolution. In such a case, the notion of a quasi-equilibrium ensemble of sub-grid-scale processes, upon which all current parameterizations schemes are based, cannot be a fully-appropriate concept for representing

the actual parameterized heating (Palmer, 1997). For example, even if the parameterized heating fields agree on average (*i.e.* over many time steps) at the chosen grid point, there must inevitably be some standard deviation in the time-step by time-step difference between observed and modeled heating.

Since October 1998, a simple stochastic scheme for simulating random model errors due to parameterized physical processes has been used in the ECMWF EPS (Buizza *et al.*, 1999). The scheme is based on the notion that the sort of random error in parameterized forcing are coherent between the different parameterization modules, and have certain coherence on the space and time scales associated, for example, with organized convection schemes. Moreover, the scheme assumes that the larger the parameterized tendencies, the larger the random error component will be. The notion of coherence between modules allows the stochastic perturbation to be based on the total tendency from all parameterized processes, rather than on the parameterized tendencies from each of the individual modules. In this respect the ECMWF scheme differs conceptually from that of Houtekamer *et al.* (1996). More details about the scheme are reported in the following section.

5. – The ECMWF ensemble prediction system

Routine real-time execution of the ECMWF EPS started in December 1992 with a 33-member T63L19 configuration (spectral triangular truncation T63 and 19 vertical levels, Palmer *et al.*, 1993, Molteni *et al.*, 1996). A major upgrade to a 51-member $\mathrm{T_L}159\mathrm{L}31$ system (spectral triangular truncation T159 with linear grid) took place in 1996 (Buizza *et al.*, 1998). A scheme to simulate model uncertainties due to random model error in the parameterized physical processes was introduced in 1998. A second major resolution upgrade took place on the 21st of November 2000, when the EPS resolution was increased from $\mathrm{T_L}159\mathrm{L}31$ to $\mathrm{T_L}255\mathrm{L}31$, which is equivalent to a grid-point spacing of about 80 km.

5˙1. *The original* EPS *configuration: initial perturbations only.* – Schematically, each ensemble member e_j was defined by the time integration

$$e_j(t) = \int_{t=0}^{t} \big[A(e_j, t) + P(e_j, t)\big]\,\mathrm{d}t \tag{2}$$

of the model equations

$$\frac{\partial e_j}{\partial t} = A(e_j, t) + P(e_j, t), \tag{3}$$

starting from perturbed initial conditions

$$e_j(t=0) = e_0(t=0) + \delta e_j(t=0), \tag{4}$$

where A and P identify the contribution to the full equation tendency of the non-parameterized and parameterized physical processes, and where $e_0(t = 0)$ is the operational analysis at $t = 0$.

The initial perturbations $\delta e_j(t = 0)$ were generated using the singular vectors of the linear version of the ECMWF, computed to maximize the total energy norm over a 48-hour time interval (Buizza and Palmer, 1995), and scaled to have an amplitude comparable to analysis error estimates.

The singular vectors of the tangent forward propagator sample the phase space directions of maximum growth during a 48-hour time interval. Small errors in the initial conditions along these directions would amplify most rapidly, and affect the forecast accuracy. The reader is referred to appendix A for a more complete mathematical definition of the singular vectors.

Figure 8 illustrates the typical structure of the leading singular vector used to generate the ensemble of initial perturbations for 17 January 1997. The left panels show the singular vector at initial time, and the right panels at final time at two levels, 500 hPa (top) and 700 hPa (bottom). This singular vector has been computed using a total energy norm (see appendix A for details). Total energy singular vectors are usually located in the lower troposphere at initial time, with total energy peaking at between around 700 hPa (*i.e.* around 3000 m), in regions of strong barotropic and baroclinic energy conversion (Buizza and Palmer, 1995). During their growth, they show an upscale energy transfer and upward energy propagation (Hartmann *et al.*, 1995). Figure 8 confirms this behavior: the amplitude is larger at 700 hPa than at 500 hPa at initial time, but the amplitude at the two levels is similar at final time. Figure 8 also shows that the singular vector has larger scale at the final than at the initial time.

Results published in the literature (Buizza and Palmer, 1995) have indicated a very good agreement between the regions where singular vectors are located and other measures of baroclinic instability such as the Eady index introduced by Hoskins and Valdes (1990). The Eady index

$$\sigma_{\mathrm{E}} = 0.31 \frac{f}{N} \frac{\mathrm{d}u}{\mathrm{d}z} \tag{5}$$

is an expression for the growth rate of the most unstable Eady mode, and can be considered as a measure of the level of baroclinic instability of the atmosphere. In eq. (5) the static stability N and the vertical wind shear $\mathrm{d}u/\mathrm{d}z$ (u is the wind magnitude) can be estimated using the 300 and 1000 hPa potential temperature. Figure 9 shows the agreement between the singular vectors geographical distribution and the Eady index for singular vectors growing between 12 UTC of 17 and 19 January 1997. The reader is referred to Hoskins *et al.* (2000) for a discussion of the nature of singular vector growth and structure in terms of basic theoretical concepts.

The EPS 50 perturbed initial conditions were generated by adding and subtracting 25 perturbations defined using 25 singular vectors selected from computed singular vectors so that they do not overlap in space. The selection criteria were that the leading 4 singular vectors are always selected, and that subsequent singular vectors are selected only if less than 50% of their total energy cover a geographical region where already 4 singular vectors are located.

Once the 25 singular vectors were selected, an orthogonal rotation in phase-space and a final re-scaling were performed to construct the ensemble perturbations. The purpose of the phase-space rotation is to generate perturbations with the same globally averaged energy as the singular vectors, but smaller local maxima and a more uniform spatial distribution. Moreover, unlike the singular vectors, the rotated singular vectors are characterized by similar amplification rates (at least up to 48 hours). Thus, the rotated singular vectors diverge, on average, equally from the control forecast. The rotation is defined to minimize the local ratio between the perturbation amplitude and the amplitude of the analysis error estimate given by the ECMWF data assimilation procedure.

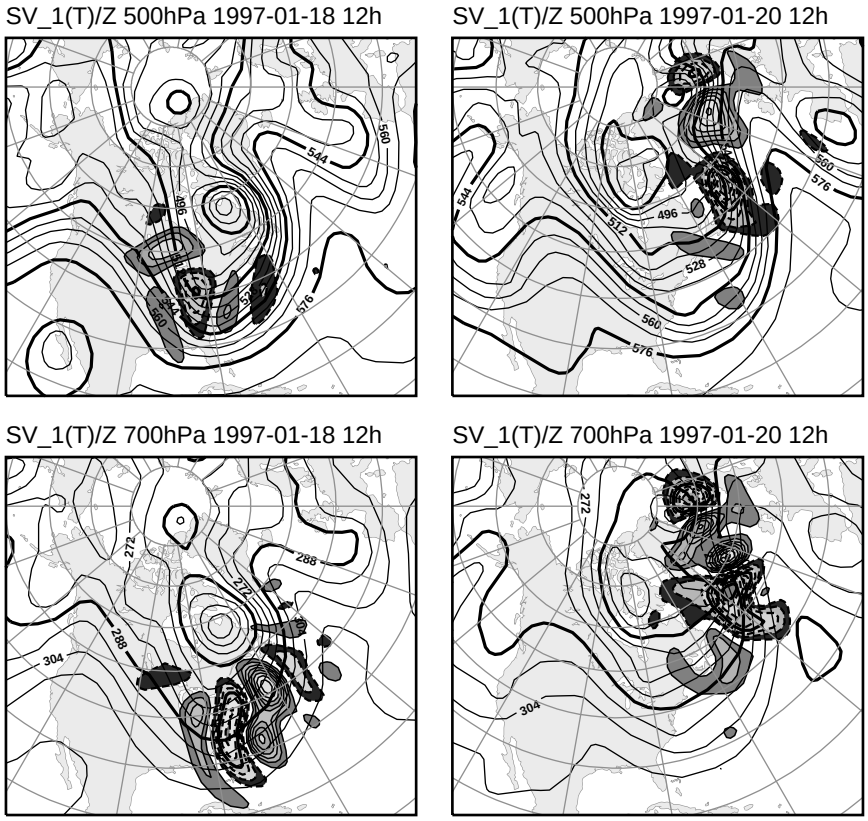

Fig. 8. – Most unstable singular vector growing between 17 and 19 January 1997 at initial (left panels) and final (right panels) times. The top panels show the singular vector temperature component (gray-shading with solid contour lines for positive and gray-shading with dashed contour lines for negative values) and the atmospheric state (geopotential height) at 500 hPa (*i.e.* approximately at 5000 m). Bottom panels are as top panels but for 700 hPa (*i.e.* approximately at 3000 m). Contour interval is 8 dam for geopotential height, and 0.2 degrees for temperature at initial time and 1.0 degree at final time.

Until 26 March 1998, the EPS initial perturbations were computed to sample instabilities growing in the forecast range, and no account was taken of perturbations that had grown during the data assimilation cycle leading up to the generation of the initial conditions (Molteni *et al.*, 1996). A way to take into account perturbations growing during the data assimilation period was to generate the EPS initial perturbation using two sets of singular vectors. In mathematical terms, since 26 March 1998 (Barkmeijer *et al.*, 1999) the day d initial perturbations have been generated using both the singular vectors growing in the forecast range between day d and day $d+2$ at initial time, and the singular vectors that had grown in the past between day $d-2$ and day d at final time

$$\delta e_j(t=0) = \sum_{i=1}^{25} \left[\alpha_{i,j} v_i^{d,d+2}(t=0) + \beta_{i,j} v_i^{d-2,d}(t=48\text{ h})\right], \tag{6}$$

where $v_i^{d,d+2}(t=0)$ is the i-th singular vector growing between day d and $d+2$ at time

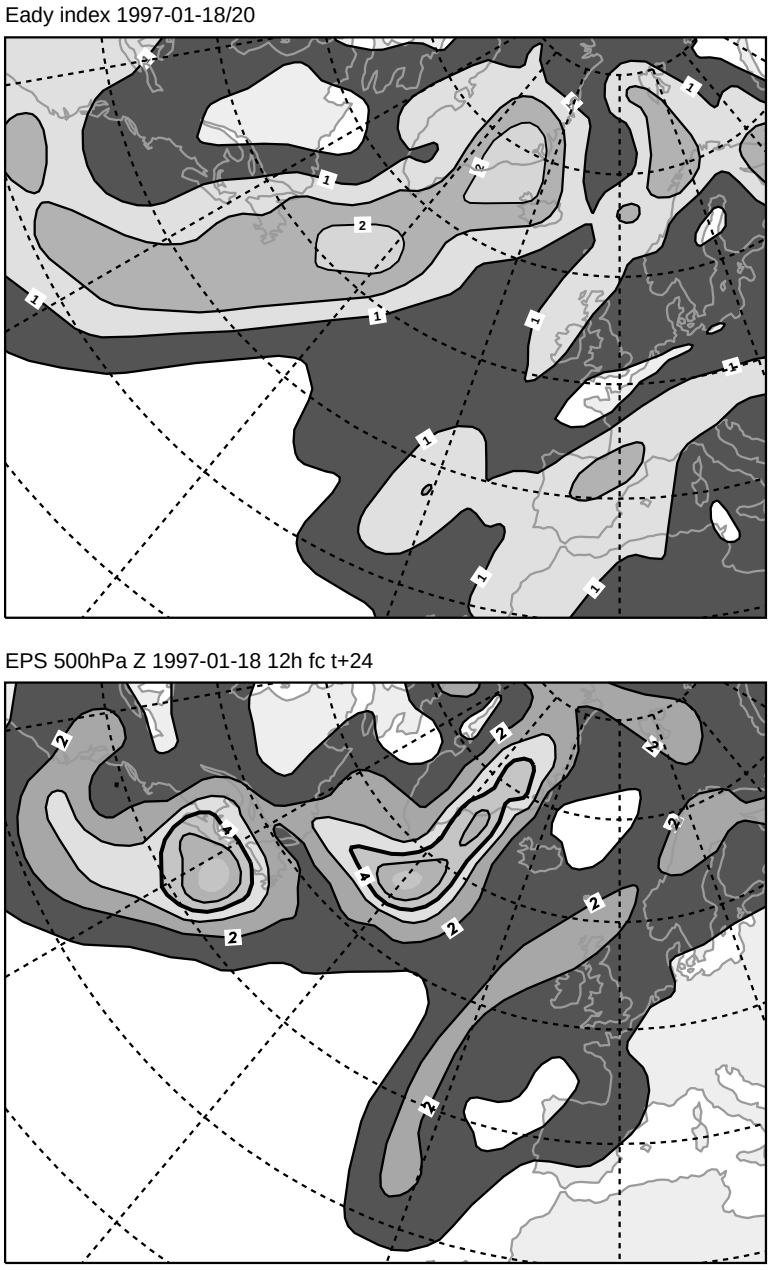

Fig. 9. – Eady index (top panel) and location of the leading singular vectors identified by the root-mean-square amplitude of the EPS perturbations at forecast day 1 (bottom panel) for the case of 17 January 1997. Contour interval is $1\,\mathrm{day}^{-1}$ for the Eady index, and 1 m for the EPS perturbation amplitude.

$t = 0$. The coefficients $\alpha_{i,j}$ and $\beta_{i,j}$ set the initial amplitude of the ensemble perturbations, and are defined by comparing the singular vectors with estimates of analysis

errors (Molteni *et al.*, 1996). Furthermore, the coefficients $\alpha_{i,j}$ and $\beta_{i,j}$ are set so that on average the ensemble standard deviation (which is a measure of the average distance of a single member from the ensemble mean) is comparable to the error of the ensemble-mean (which is a measure of the distance of the analysis from the ensemble mean). This gurantees that, on average, the analysis has the same distance from the ensemble mean as a perturbed member.

The initial perturbations are specified in terms of the spectral coefficients of the 3-dimensional vorticity, divergence and temperature fields (no perturbations are defined for the specific humidity since the singular vector computation is performed with a dry linear forward/adjoint model), and of the 2-dimensional surface pressure field. They are added and subtracted to the control initial conditions to define perturbed initial conditions. Then, $50 + 1$ (control) 10 day non-linear integrations are performed.

5˙2. *Simulation of random model errors in the* ECMWF EPS. – In October 1998, a scheme to simulate random model errors due to parameterized physical processed was introduced (Buizza *et al.*, 1999). This scheme can be considered as a simple first attempt to simulated random model errors due to parametrized physical processes. It is based on the notion that random errors due to parametrized physical processes are coherent between the different parametrization modules and have a certain coherence on the space and time scales represented by the model. The scheme assumes that the larger the parametrized tendencies, the larger the random error component.

In the new EPS, each ensemble member e_j can be seen as the time integration

$$e_j(t) = \int_{t=0}^{t} \left[A(e_j, t) + P'_j(e_j, t)\right] \mathrm{d}t \tag{7}$$

of the perturbed model equations

$$\frac{\partial e_j}{\partial t} = A(e_j, t) + P'_j(e_j, t) \tag{8}$$

starting from the perturbed initial conditions defined in eq. (1), where A and P' identify the contribution to the full equation tendency of the non-parameterized and parameterized physical processes. For each grid point $x = (\lambda, \phi, \sigma)$ (identified by its latitude, longitude and vertical hybrid coordinate), the perturbed parameterized tendency (of each state vector component) is defined as

$$P'_j(e_j, t) = \left[1 + \left\langle r_j(\lambda, \phi, t)\right\rangle_{D,T}\right] P(e_j, t), \tag{9}$$

where P is the unperturbed diabatic tendency, and $\langle\cdot\cdot\rangle_{D,T}$ indicates that the same random number r_j has been used for all grid points inside a $D \times D$ degree box and over T time steps.

The notion of space-time coherence assumes that organized systems have some intrinsic space and time-scales that may span more than one model time step and more than one model grid point. Making the stochastic uncertainty proportional to the tendency is based on the concept that organization (away from the notion of a quasi-equilibrium ensemble of sub-grid processes) is likely to be stronger, the stronger is the parameterized contribution. A certain space-time correlation is introduced in order to have tendency perturbations with the same spatial and time scales as observed organization.

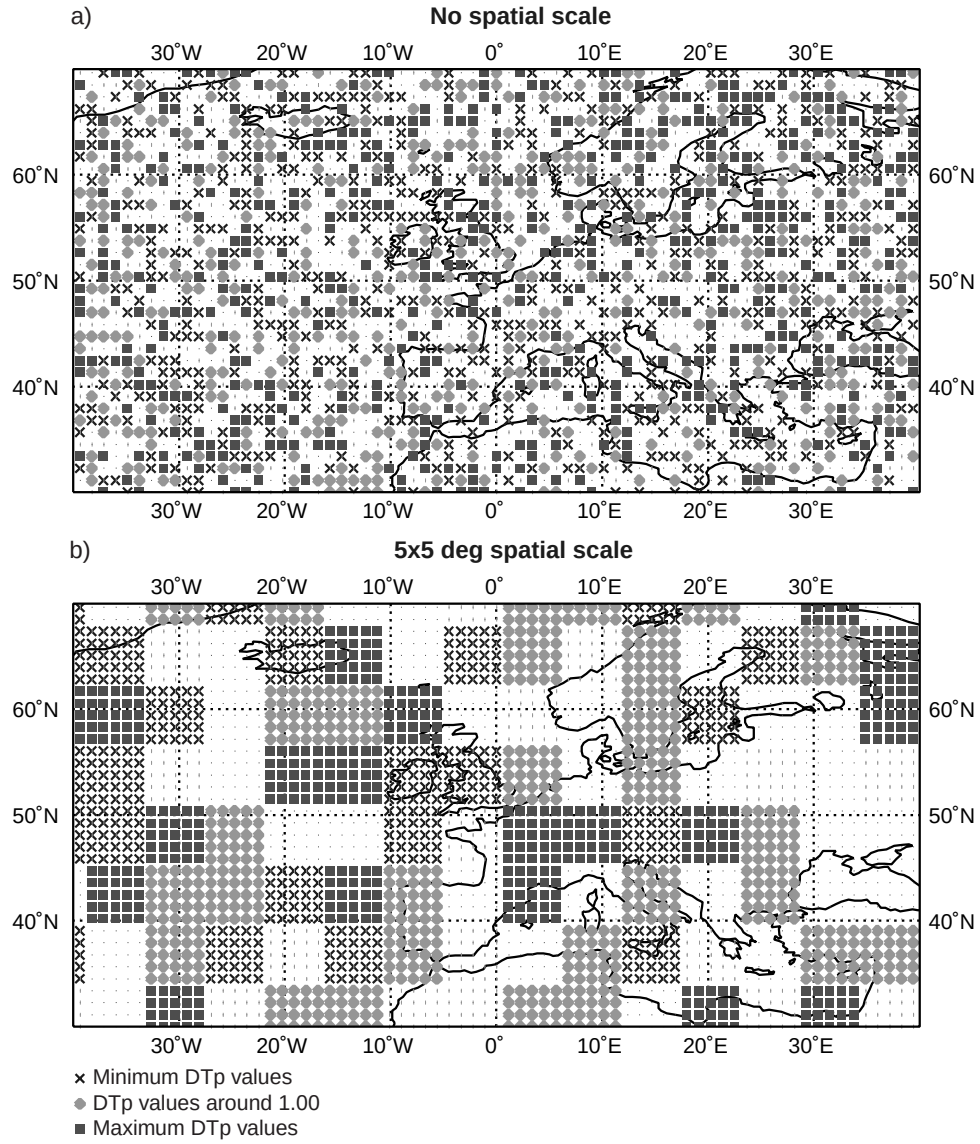

Fig. 10. – Random numbers used to perturb the tendencies due to parameterised physical processes. Panel a) shows the case of no spatial scale, in other words when different random numbers are used at each grid point. Panel b) shows the case when the same random number was used for grid points inside 5-degree boxes. Crosses identify grid points with random numbers $-0.5 \leq r_j \leq -0.3$, diamonds points with $-0.1 \leq r_j \leq 0.1$, and squares points with $0.3 \leq r_j \leq 0.5$.

Figure 10 shows a map of the random numbers used in a configuration tested when developing the so-called stochastic physics scheme. Figure 10a shows the matrix of random numbers r_j when each grid point was assigned an independent value, while fig. 10b shows the matrix when the same random number was used inside 5-degree boxes.

Results indicated that even perturbations without any spatial structure (*i.e.* with random numbers as in fig. 10a) had a major impact on 10 day model integrations (Buizza *et al.*, 1999). On 21 October 1998, following extensive experimentation, the stochastic physics scheme has been implemented in the operational EPS with random numbers sampled uniformly in the interval $[-0.5, 0.5]$, a 10- degree box size ($D = 10$), and a 6 hours time interval ($T = 6$).

Mullen and Buizza (2001) compared the accuracy of the EPS precipitation prediction over the United States for the period 1 January 1997 to 31 January 1999. They concluded that the implementation of stochastic physics appears to have raised short-range skill for thresholds between 1–20 mm during winter.

6. – Targeted observations

Consider a meteorological system evolving between time t_0 and t, localised at final time t inside a geographical area σ_t (hereafter verification area). Suppose that extra observations could be taken inside a geographical area σ_0 at initial time t_0 (hereafter target area), with the purpose of improving the time t forecast inside σ.

Singular vectors with maximum energy at final time inside a verification area can be used to identify the target area where extra observation should be taken, at initial time, to reduce the forecast error inside the verification area itself (Buizza and Montani, 1999). The reader is referred to appendices A and B for a more complete description of the mathematical formulation.

Other strategies can be used to target adaptive observations. Langland and Rohaly (1996), following the work of Rabier *et al.* (1996) on sensitivity vectors, proposed to use the lower tropospheric vorticity of the forecast state as cost function, and to target the region where the sensitivity field is maximum. A similar technique, but based on the use of a quasi-inverse linear model, was proposed by Pu *et al.* (1997, 1998). Bishop and Toth (1999) introduced the Ensemble Transform technique, in which linear combinations of ensemble perturbations are used to estimate the prediction error variance associated with different possible deployments of observational resources (see Bishop *et al.*, 2000 for theoretical aspects of this technique). Finally, following Hoskins *et al.* (1985) and Appenzeller *et al.* (1996), a more subjective strategy based on the use of potential vorticity to analyse atmospheric was also developed.

All these techniques were applied to target observations for the first time during FASTEX, the Fronts and Atlantic Storm Track Experiment (Joly *et al.*, 1996, Thorpe and Shapiro, 1995, Snyder, 1996).

The focus of the FASTEX campaign was the extra-tropical cylonic storms that form over the western and mid Atlantic Ocean, and take about 2 days to develop and move towards Europe. Forecast failures are often associated with these very active atmospheric phenomena.

Figure 11 shows the tracks of one of the storms observed during FASTEX, IOP 17 (IOP stands for Intensive Observation Period), and the location of various aircrafts that made additional observations between 17 and 19 February 1997 (Montani *et al.*, 1999). Singular vectors, computed to have maximum total energy inside a verification region centred on the British Isles, were used to identify the most sensitive regions where observations were made. The comparison of the central pressure of two forecasts, one started from initial conditions computed with and one without the extra observations, with the observed value (fig. 12) indicates that additional, targeted observations can improve the

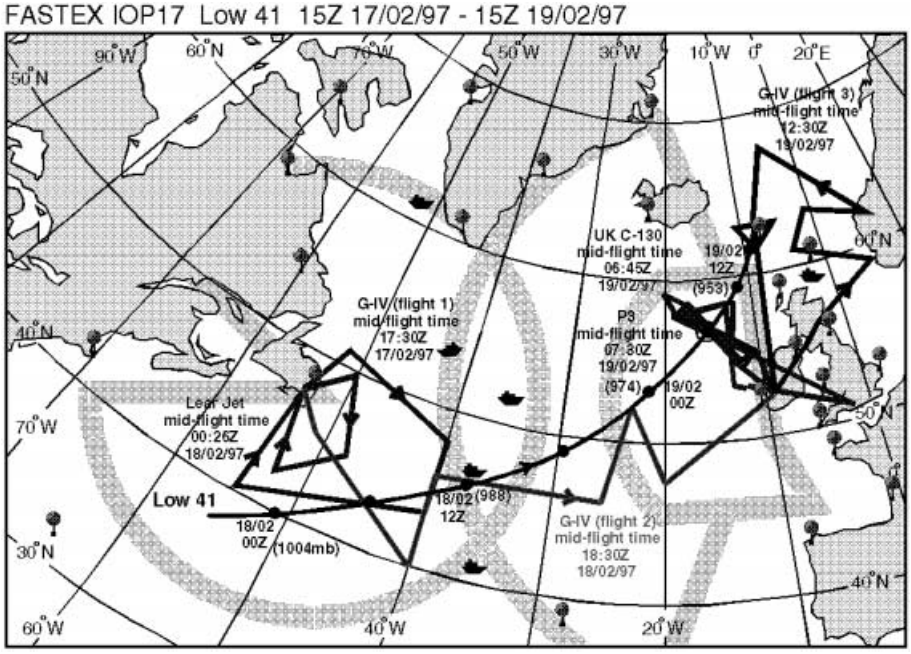

Fig. 11. – Map summarising the extra observations taken during the FASTEX experiment for IOP 17. The solid track with full-black circles (with lables listing the date, time and MSLP pressure) identifies the location of the cyclone minimum pressure; the solid lines with arrows starting either from New Foundland (52W, 47N) and from Ireland identify the aircraft missions; the balloon and ship symbols indicate the location of additional radio-soundings (from Montani *et al.*, 1999).

forecast accuracy. Figure 13 shows the average impact of the targeted observations on the forecast error. Results indicated up to 20% forecast error reduction.

After FASTEX, NORPEX-98, the North Pacific Experiment (Langland *et al.*, 1999) and CALJET, the California Land-falling Jets experiments (Emanuel *et al.*, 1995, Dabbert *et al.*, 1996) had been realised. Results from all these experiments confirmed that taking extra observations in sensitive regions could reduce forecast errors. Other similar field experiments are been planned to take place over the US (see `http://box.mmm.ucar.edu/uswrp/fieldprojects/fieldprojects.html`). PACJET (Pacific Landfalling Jets Experiment) has been planned for Jan-Feb 2001 to develop and test methods to improve short-term (0–24 hour) forecasts of damaging weather on the US West Coast. THORPEX (The Hemispheric Observing system Research and Predictability Experiment) is planned as a 5–10 years international research program to test the hypothesis that 2 to 10 day numerical forecasts of high-impact weather events can be significantly improved by adding high-quality observations in critical areas of the extra-tropical oceanic storm-tracks and other data-sparse remote areas.

It is still unclear whether a best targeting technique can be defined, whereby "best" means that will lead to the largest forecast error reduction. In fact, it is impossible to define the best targeting technique without considering the metric used to assess the forecast error. As discussed in mathematical terms in appendices A, B, the metric defines the problem, and one technique could be best according to one metric (*e.g.*, root-mean-square

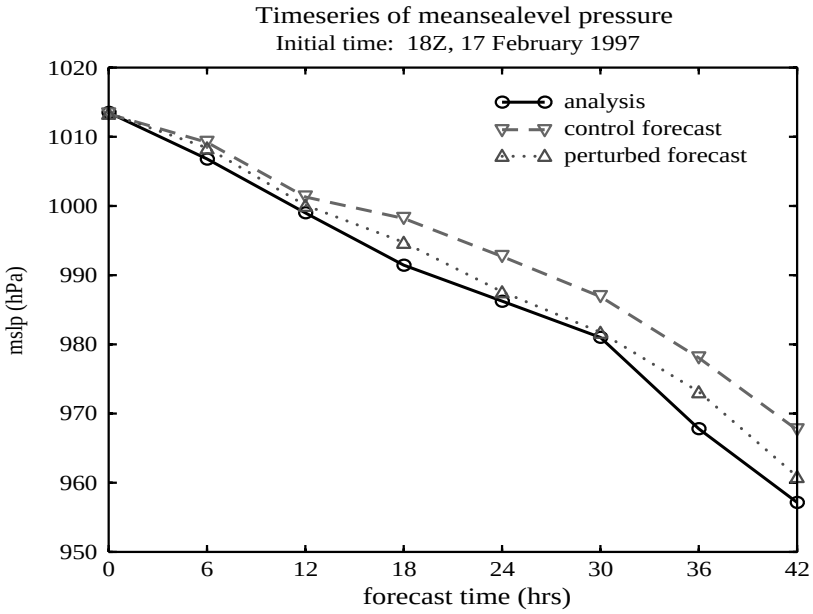

Fig. 12. – 6-hourly time series of the cyclone central pressure forecast without (dashed line) and with (dotted line) extra observations, and observed (solid line), for IOP 17 (from Montani *et al.*, 1999).

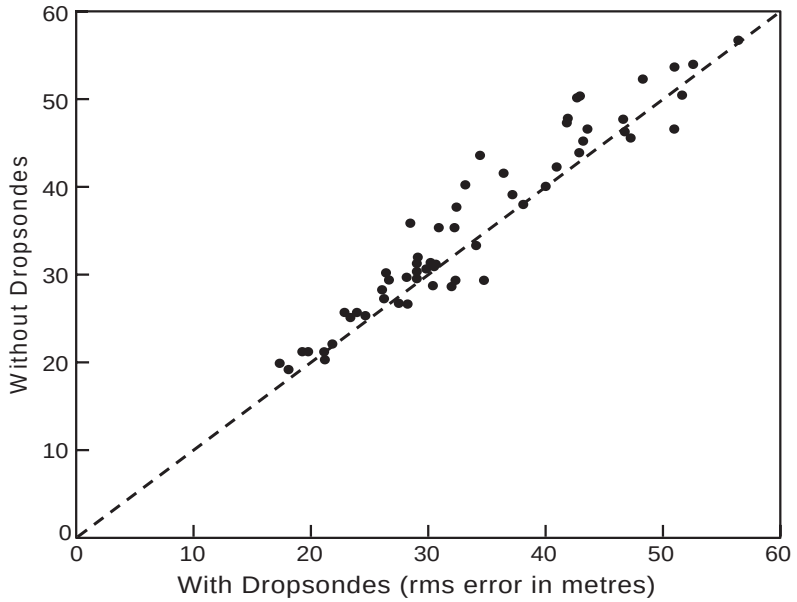

Fig. 13. – Scatter plot of the mean forecast errors with (x-axis) and without (y-axis) the extra observations, for the 500 and 1000 hPa geopotential height fields over Europe and North Atlantic at forecast day 2, 2.5 and 3 (from Montani *et al.*, 1999).

error of mean-sea-level-pressure predictions) but not according to another one (*e.g.*, total energy, or precipitation mean absolute error). Despite this, it is anyway interesting to compare different targeting techniques to gauge the range of variability among targets computed following different procedures. Majumdar *et al.* (2001) compare targets computed using the Ensemble Transform Kalman Filter Technique (Bishop and Toth, 1999) and ECMWF and NRL singular vectors (Buizza and Montani, 1999, Gelaro *et al.*, 1999) for 10 cases during the NORPEX 1998 field experiment. They show summary maps and highlight similarities/differences between the different targets, but they explicitly encourage the readers to draw their own conclusions. They conclude that the three targets have strong large-scale similarities but have significantly different small-scale features.

Robotic aerosondes capable of long-range monitoring could be used operationally in a very near future to fill chronic gaps in the global upper-air sounding network (Holland *et al.*, 1992), and take extra observations in objectively identified regions. This follows years of intensive research at the Bureau of Meteorology of Melbourne, Australia, that culminated with the first-ever unmanned aircraft crossing of the Atlantic Ocean in August 1998 (`http://www.aerosonde.com/opshist.htm`).

7. – Summary and future developments

Two of the most important advances in numerical weather prediction of the last 10 years, the operational implementation of ensemble prediction systems and the development of objective techniques to target adaptive observations, have been discussed.

Ensemble systems provide a possible way to estimate the probability distribution function of forecast states. Results have demonstrated that a probabilistic approach to weather prediction can provide more information than a deterministic approach based on a single, deterministic forecast.

Ensemble prediction systems are particularly useful, if not necessary, to provide early warnings of extreme weather events (Buizza and Hollingsworth, 2000). Ensemble systems can be used to predict probabilities of intense precipitation events (fig. 14). Ensemble-based probabilistic predictions can be used to optimise business activities (Taylor and Buizza, 2001). Global ensemble systems can be used to provide boundary and initial conditions for higher-resolution, limited-area ensemble prediction systems (Molteni *et al.*, 2001, Marsigli *et al.*, 2001).

At ECMWF, work is in progress in many different areas to further improve the current ensemble prediction system.

Linearized versions of the most important physical processes have been developed (Mahfouf, 1999), and investigation into the behaviour of the linear models in the computation of tropical singular vectors has started. The tropical target area has been chosen because the current EPS lacks perturbations of the initial condition in this area, where moist processes are of key importance. Results (Barkmeijer *et al.*, 2001, Puri *et al.*, 2001) indicate that the inclusion of tropical singular vectors is essential in cases of hurricane prediction. Results indicate that tropical singular vectors are needed to generate a realistic spread among the ensemble of hurricane tracks.

The operational initial perturbations of the ECMWF EPS are constructed using singular vectors with maximum total energy growth. Total energy singular vectors have no knowledge of analysis error statistics. Generally speaking, it would be desirable to use information about analysis error characteristics in the singular vector computation. One way of improving upon this is to use in the singular vector computation statistics generated by the data assimilation system. Work is in progress to use the Hessian of

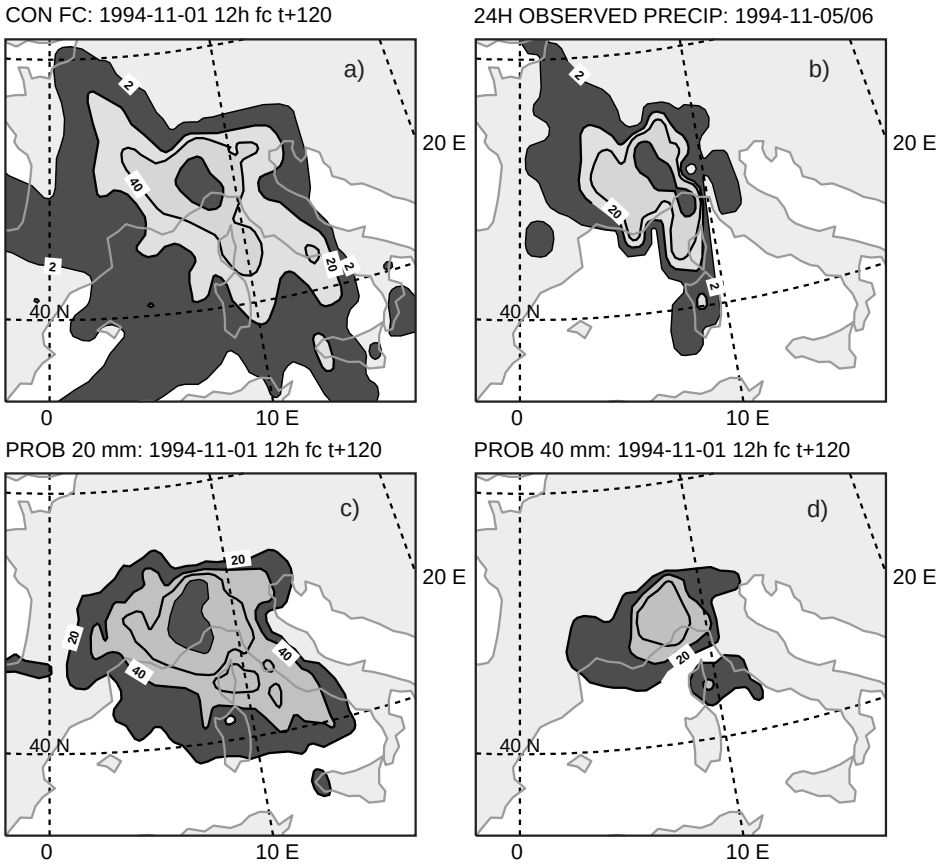

Fig. 14. – High-resolution $T_L319L31$ forecasts for the flood in Piemonte, Italy, 5-6 November 1994. (a) Precipitation forecast, accumulated between $t + 96$ h and $t + 120$ h, predicted by the control forecast. (b) Observed precipitation field. (c) Ensemble probability forecast of more than 20 mm/d of precipitation. (d) Ensemble probability forecast of more than 40 mm/d of precipitation. Contour isolines 2, 20, 40 and 100 mm/d for precipitation, and every 20% for probabilities.

the cost function of the 3-dimensional (or 4-dimensional) variational assimilation system (3D/4D-Var) to define singular vectors (Barkmeijer *et al.*, 1998). These so-called Hessian singular vectors are constrained at initial time by analysis error statistics but still produce fast perturbation growth during the first few days of the forecast.

Work is in progress to investigate whether a so-called consensus analysis, defined as the average of analyses produced by different weather centres, is a better estimate of the atmospheric initial state than the ECMWF analysis (Richardson, 2000, personal communication). The operational EPS configuration has been run from the consensus analysis, average of the ECMWF, UKMO (UK Meteorological Office), Météo-France, NCEP (National Centers for Environmental Prediction, Washington) and DWD (Deutscher WetterDienst, Offenbach) analyses. The same perturbations as used in the operational EPS have been added to the consensus analysis to create the 50 perturbed initial conditions. Preliminary results show that the skill of the control forecast is improved if the consensus

analysis is used instead of the ECMWF analysis as the unperturbed initial condition. Results also indicate that the difference between the spread in the two systems is rather small, while the ensemble-mean forecast of the system started from the consensus analysis is more skilful.

The quantitative evaluation of ensemble systems should be based on the comparison of the forecast PDF with the observed PDF, and verification measures should be designed to assess the statistical consistency and usefulness of the predicted PDF (Talagrand *et al.*, 1999; Buizza, 1997, 2001). These two properties should be verified by considering not only first-order (ensemble mean) but also second-order (ensemble standard deviation) moments of the predicted PDF and the second-order moment, and should be performed both a grid point level and considering large-scale atmospheric patterns (Molteni and Buizza, 1999). The reader is referred to Wilks (1995) for a review of commonly used accuracy and verification measures. New measures have been developed to assess the potential economic value of ensemble prediction (Richardson, 2000, Buizza, 2000). These measures are defined by coupling contingency tables and costloss decision models (Katz *et al.*, 1982, Wilks and Hamill, 1995).

At ECMWF, an ensemble approach to data assimilation is under investigation (Buizza and Palmer, 1998). Following Houtekamer *et al.* (1996), but with the ECMWF approach to represent model uncertainties, work has started at ECMWF to generate an ensemble of initial perturbations using the ECMWF 3D/4D-Var data assimilation. The purpose of this work is to investigate whether a better estimate of the "true" state of the atmosphere can be computed using this probabilistic approach.

The weather is a chaotic system, and numerical weather prediction is a very difficult task. This work has shown that the application of linear algebra (*i.e.* the use of singular vectors computed by solving an eigenvalue problem defined by the tangent forward and adjoint versions of the model) to meteorology can help in designing new ways to numerical weather prediction (Buizza, 1997). The same technique can be applied to any dynamical system, in particular to very complex systems with large dimensions.

* * *

The ECMWF Ensemble Prediction System is the result of the work of many ECMWF staff members and consultants. It is based on the Integrated Forecasting System/Arpege software, developed in collaboration by ECMWF and Meteo-France. The work of many ECMWF and Meteo-France staff and consultants is acknowledged. I am grateful to R. Hine for all his editorial help.

Appendix A.

Singular vector definition

Farrell (1982), studying the growth of perturbations in baroclinic flows, showed that, although the long time asymptotic behavior is dominated by discrete exponentially growing normal modes when they exist, physically realistic perturbations could present, for some finite time intervals, amplification rates greater than the most unstable normal mode amplification rate. Subsequently, Farrell (1988, 1989) showed that perturbations with the fastest growth over a finite time interval could be identified solving the eigenvalue problem of the product of the tangent forward and adjoint model propagators. His results supported earlier conclusions by Lorenz (1965) that perturbation growth in realistic models is related to the eigenvalues of the operator product.

Kontarev (1980) and Hall and Cacuci (1983) first used the adjoint of a dynamical model for sensitivity studies. Later on, Le Dimet and Talagrand (1986) proposed an algorithm, based on an appropriate use of an adjoint dynamical equation, for solving constraint minimization problems in the context of analysis and assimilation of meteorological observations. More recently, Lacarra and Talagrand (1988) applied the adjoint technique to determine optimal perturbations using a simple numerical model. Following Urban (1985) they used a Lanczos algorithm (Strang, 1986) in order to solve the related eigenvalue problem. For a bibliography in chronological order of published works in meteorology dealing with adjoints up to the end of 1992, the reader is referred to Courtier *et al.* (1993).

After Farrell and Lorenz, calculations of perturbations growing over finite-time intervals were performed, for example, by Borges and Hartmann (1992) using a barotropic model, and by Molteni and Palmer (1993) using a barotropic and a 3-level quasi-geostrophic model at spectral triangular truncation T21. Buizza (1992) and Buizza *et al.* (1993) first identified singular vectors in a primitive equation model with a large number of degrees of freedom.

Let χ be the state vector of a generic autonomous system, whose evolution equations can be formally written as

$$\frac{\partial \chi}{\partial t} = A(\chi). \tag{A.1}$$

Denote by $\chi(t)$ an integration of eq. (A.1) from t_0 to t which generates a trajectory from an initial point χ_0 to $\chi_1 = \chi(t)$. The time evolution of a small perturbation x around the time evolving trajectory $\chi(t)$ can be described, in a first approximation, by the linearized model equations

$$\frac{\partial x}{\partial t} = A_l x\,, \tag{A.2}$$

where $A_l = (\partial A(x)/\partial x)|_{\chi(t)}$ is the tangent operator computed at the trajectory point $\chi(t)$.

Let $L(t, t_0)$ be the integral forward propagator of the dynamical eq. (A.2) linearized about a non-linear trajectory $\chi(t)$

$$x(t) = L(t, t_0)x(t_0), \tag{A.3}$$

that maps a perturbation x at initial time t_0 to the optimization time t. The tangent forward operator L maps the tangent space Π_0, the linear vector space of perturbations at χ_0, to Π_0, the linear vector space at χ_1.

Consider two perturbations x and y, *e.g.*, at χ_0, a positive definite Hermitian matrix E, and define the inner product $(\cdot\cdot;\cdot\cdot)_E$ as

$$(x; y)_E = \langle x; Ey\rangle \tag{A.4}$$

on the tangent space Π_0 in this case, where $\langle\cdot\cdot;\cdot\cdot\rangle$ identifies the canonical Euclidean scalar product,

$$\langle x; y\rangle = \sum_{i=1}^{N} x_i y_i. \tag{A.5}$$

Let $\|\cdot\cdot\|_E$ be the norm associated with the inner product $(\cdot\cdot;\cdot\cdot)_E$,

$$\|x\|_E^2 = (x;x)_E = \langle x; Ex\rangle. \tag{A.6}$$

Let L^{*E} be the adjoint of L with respect to the inner product $(\cdot\cdot;\cdot\cdot)_E$,

$$\left(L^{*E}x; y\right)_E = (x; Ly)_E. \tag{A.7}$$

The adjoint of L with respect to the inner product defined by E can be written in terms of the adjoint L^* defined with respect to the canonical Euclidean scalar product,

$$L^{*E} = E^{-1}L^*E. \tag{A.8}$$

From eqs. (A.3) and (A.8) it follows that the squared norm of a perturbation x at time t is given by

$$\|x(t)\|_E^2 = \left(x(t_0); L^{*E}Lx(t_0)\right)_E. \tag{A.9}$$

Equation (A.9) shows that the problem of finding the phase space directions x for which $\|x(t)\|_E^2/\|x(t_0)\|_E^2$ is maximum can be reduced to the search of the eigenvectors $v_I(t_0)$

$$L^{*E}Lv_i(t_0) = \sigma_i^2 v_i(t_0) \tag{A.10}$$

with the largest eigenvalues σ_i^2.

The square roots of the eigenvalues, σ_i, are called the singular values and the eigenvectors $v_i(t_0)$ the (right) singular vectors of L with respect to the inner product E (see, *e.g.*, Noble and Daniel, 1977). The singular vectors with largest singular values identify the directions characterized by maximum growth. The time interval $t - t_0$ is called optimization time interval.

Unlike L itself, the operator $L^{*E}L$ is normal. Hence, its eigenvectors $v_I(t_0)$ can be chosen to form a complete orthonormal basis in the N-th dimensional tangent space of the perturbations at χ_0. Moreover, the eigenvalues are real, $\sigma_i^2 \geq 0$.

At optimization time t, the singular vectors evolve to

$$v_i(t) = L(t, t_0)v_i(t_0), \tag{A.11}$$

which in turn satisfy the eigenvector equation

$$LL^{*E}v_i(t) = \sigma_i^2 v_i(t). \tag{A.12}$$

From eqs. (A.9) and (A.12) it follows that

$$\|v_i(t)\|_E^2 = \sigma_i^2. \tag{A.13}$$

Since any perturbation $x(t)/\|x(t_0)\|_E$ can be written as a linear combination of the singular vectors $v_I(t)$, it follows that

$$\max_{\|x(t_0)\|_E \neq 0} \left(\frac{\|x(t)\|_E}{\|x(t_0)\|_E} \right) = \sigma_i. \tag{A.14}$$

Thus, maximum growth as measured by the norm $\|\cdot\cdot\|_E$ is associated with the dominant singular vector v_1.

Given the tangent forward propagator L, it is evident from eq. (A.10) that singular vectors' characteristics depend strongly on the inner product definition and to the specification of the optimization time interval.

The problem can be generalized by selecting a different inner product at initial and optimization time. Consider two inner products defined by the (positive definite Hermitian) matrices E_0 and E, and re-state the problem as finding the phase space directions x for which

$$\frac{\|x(t)\|_E}{\|x(t_0)\|_{E_0}} = \frac{\langle Lx(t_0); ELx(t_0)\rangle}{\langle x(t_0); E_0 x(t_0)\rangle} \tag{A.15}$$

is maximum. Applying the transformation $y = E_0^{1/2}x$, the right hand side of eq. (A.15) can be transformed into

$$\frac{\langle LE_0^{-1/2}y(t_0); ELE_0^{-1/2}y(t_0)\rangle}{\langle y(t_0); y(t_0)\rangle} = \frac{\langle y(t_0); E_0^{-1/2}L^*ELE_0^{-1/2}y(t_0)\rangle}{\langle y(t_0); y(t_0)\rangle}. \tag{A.16}$$

Since

$$E_0^{-1/2}L^*ELE_0^{-1/2} = \left(E^{-1/2}LE_0^{-1/2}\right)^*\left(E^{-1/2}LE_0^{-1/2}\right), \tag{A.17}$$

the phase space directions which maximize the ratio in eq. (A.16) are the singular vectors of the operator $E^{-1/2}LE_0^{-1/2}$ with respect to the canonical Euclidean inner product. With this definition, the dependence of the singular vectors' characteristics on the inner products is made explicit.

At ECMWF, due to the very large dimension of the system, the eigenvalue problem that defines the singular vectors is solved by applying a Lanczos code (Gelub and Van Loan, 1983).

Appendix B.

Projection operators

The set of differential equations that defines the system evolution can be solved numerically with different methods. For example, they can be solved with spectral methods, by expanding a state vector onto a suitable basis of functions, or with finite-difference methods in which the derivatives in the differential equation of motions are replaced by finite-difference approximations at a discrete set of grid points in space. The ECMWF primitive equation model solves the system evolution equations partly in spectral space, and partly in grid point space.

Denote by x_g the grid point representation of the state vector x, by S the spectral-to-grid point transformation operator, $x_g = S_x$, and by Gx_g the multiplication of the vector x_g, defined in grid point space, by the function $g(s)$:

$$g(s) = 1 \quad \forall s \in \Sigma, \qquad g(s) = 0 \quad \forall s \notin \Sigma, \tag{B.1}$$

where s defines the coordinate of a grid point, and Σ is a geographical region.

Define the function $w(n)$ in spectral space as

$$w(n) = 1 \quad \forall n \in \Omega, \qquad w(n) = 0 \quad \forall n \notin \Omega, \tag{B.2}$$

where n identifies a wave number and Ω is a sub-space of the spectral space.

Consider a vector x. The application of the local projection operator T defined as

$$T = S^{-1}GS, \tag{B.3}$$

to the vector x sets the vector x to zero for all grid points outside the geographical region Σ. Similarly, the application of the spectral projection operator W to the vector x sets to zero its spectral components with wave number outside Ω.

The projection operators T and W can be used either at initial or at final time, or at both times. As an example, these operators can be used to formulate the following problem: find the perturbations with i) the fastest growth during the time interval $t - t_0$, ii) unitary E_0-norm and wave components belonging to Ω_0 at initial time, iii) maximum E-norm inside the geographical region Σ and wave components belonging to Ω_1 at optimization time. This problem can be solved by the computation of the singular values of the operator

$$K = E^{-1/2} T S_1 L S_0 E_0^{-1/2}. \tag{B.4}$$

REFERENCES

[1] Appenzeller Ch., Davies H. C., Popovic J. M., Nickovic S. and Gavrilov M. B., *Met. Atmos. Phys.*, **58** (1996) 21-40.

[2] Barkmeijer J., van Gijzen M. and Bouttier F., *Q. J. R. Meteor. Soc.*, **124** (1998) 549, 1695-1713.

[3] Barkmeijer J., Buizza, R. and Palmer T. N., *Q. J. R. Meteor. Soc.*, **125** (1999) 2333-2351.

[4] Barkmeijer J., Buizza R., Palmer T. N., Puri K. and Mahfouf J.-F., *Q. J. R. Meteor. Soc.*, **127** (2001) 685-708.

[5] Bishop C. H. and Toth Z., *J. Atmos. Sci.*, **56** (1999) 1748-1765.

[6] Bishop C. H., Etherton B. J. and Majumdar S. J., *Mon. Wea. Rev.*, 2000, in press.

[7] Borges M. and Hartmann D. L., *J. Atmos. Sci.*, **49** (1992) 335-354.

[8] Buizza R., *Unstable Perturbations Computed Using the Adjoint Technique. ECMWF Research Department Technical Memorandum* No. 189 (ECMWF, Shinfield Park, Reading RG2 9AX, UK) 1992.

[9] Buizza R., *The singular vector approach to the analysis of perturbation growth in the atmosphere*, Ph.D. thesis, University College London, Gower Street, London, 1997.

[10] Buizza R., submitted to *Mon. Wea. Rev.*, 2000.

[11] Buizza R. and Palmer T. N., *J. Atmos. Sci.*, **52** (1995) 9, 1434-1456.

[12] Buizza R. and Montani A., *J. Atmos. Sci.*, **56** (1999) 2965-2985.

[13] Buizza R. and Palmer T. N., *Ensemble data assimilation* in *Proceedings of the 17th Conference on Weather Analysis and Forecasting, 13-17 September 1999, Denver*, (AMS) 1999, p. 241.

[14] Buizza R. and Hollingsworth A., submitted to *Meteorol. Appl.*, 2000.

[15] Buizza R., Tribbia J., Molteni F. and Palmer T. N., *Tellus*, **45A** (1993) 388-407.

[16] Buizza R., Petroliagis T., Palmer T. N., Barkmeijer J., Hamrud M., Hollingsworth A., Simmons A. and Wedi N., *Q. J. R. Meteorol. Soc.*, **124** (1998) 1935-1960.
[17] Buizza R., Miller M. and Palmer T. N., *Q. J. R. Meteorol. Soc.*, **125** (1999) 2887-2908.
[18] Charney J. G., *J. Meteor.*, **4** (1947) 135-162.
[19] Charney J. G., *Geofys. Publ.*, **17** (1948) 1-17.
[20] Courtier P. and Talagrand, *Q. J. R. Meteorol. Soc.*, **113** (1987) 1329-1347.
[21] Courtier P., Freydier C., Geleyn J.-F., Rabier F. and Rochas M., *The Arpege Project at MÉtÉo-France* in *Proceedings of the ECMWF Seminar on Numerical methods in atmospheric models*, Vol. **II** (ECMWF, Shinfield Park, Reading RG2 9AX, UK) 1991, pp. 193-231.
[22] Courtier P., Derber J., Errico R., Louis J.-F. and Vukicevic T., *Tellus*, **45A** (1993) 342-357.
[23] Courtier P., Thepaut J.-N. and Hollingsworth A., *Q. J. R. Meteorol. Soc.*, **120** (1994) 1367-1388.
[24] Dabbert W. F., Schlatter T. W., Davis C. A., Fleming R. J., Hodur R. M., Holland G. M., Koch S. E., Lord S. J., Neff W. D., Pielke Sr., R. E., Pietrafesa L. J., Raymond D., Smith R. B. and Zrni D. S., *Bull. Amer. Meteor. Soc.*, **77** (1996) 305-323.
[25] Emanuel K., Raymond D., Betts A., Bosart L., Bretherton C., Droegemeier K., Farrell B., Fritsch J. M., Houze R., Le Mone M., Lilly D., Rotunno R., Shapiro M., Smith R. and Thorpe A., *Bull. Amer. Meteor. Soc.*, **76** (1995) 1194-1208.
[26] Downton R. A. and Bell R. S., *Meteorol. Mag.*, **117** (1988) 279-285.
[27] Ehrendorfer M., *Mon. Wea. Rev.*, **122** (1994) 703-713.
[28] Ehrendorfer M. and Tribbia J. J., *Efficient prediction of covariances using singular vectors. Preprint Volume, 6th International Meeting on Statistical Climatology, Galway, Ireland, 1995*, pp. 135-138.
[29] Epstein E. S., *Tellus*, **21** (1969) 739-759.
[30] Evensen G., *J. Geoph. Res.*, **99** (1994) 10, 143-160.
[31] Farrell B. F., *J. Atmos. Sci.*, **39** (1982) 8, 1663-1686.
[32] Farrell B. F., *J. Atmos. Sci.*, **45** (2) (1988) 163-172.
[33] Farrell B. F., *J. Atmos. Sci.* **46** (9) (1989) 1193-1206.
[34] Fleming R. J., *Mon. Wea. Rev.*, **99** (1971a) 851-872.
[35] Fleming R. J., *Mon. Wea. Rev.*, **99** (1971b) 927-938.
[36] Gelaro R., Langland R. H., Rohali G. D. and Rosmond T. E., *Q. J. R. Meteorol. Soc.*, **125** (1999) 3299-3328.
[37] Gleeson T. A., *J. Appl. Meteorol.*, **9** (1970) 333-344.
[38] Golub G. H. and van Loan C. F., *Matrix Computation* (North Oxford Academic Publ. Co. Ltd.) 1983, p. 476.
[39] Hall M. C. G. and Cacuci D. G., *J. Atmos. Sci.*, **46** (1983) 9, 1193-1206.
[40] Hartmann D. L., Buizza R. and Palmer T. N., *J. Atmos. Sci.*, **52** (1995) 3885-3894.
[41] Holton J. R., *An Introduction to Dynamic Meteorology* (Academic Press Inc.) 1992.
[42] Holland G. J., McGeer T. and Youngren H., *Bull. Amer. Met. Soc.*, **73** (1992) 1987-1998.
[43] Hoskins B. J. and Valdes P. J., *J. Atmos. Sci.*, **47** (1990) 1854-1864.
[44] Hoskins B. J., McIntyre M. E. and Robertson A. W., *Q. J. R. Meteorol. Soc.*, **111** (1985) 877-946.
[45] Hoskins B. J., Buizza R. and Badger J., *Q. J. R. Meteorol. Soc.*, **126** (2000) 1565-1580.
[46] Harrison M. S. J., Palmer T. N., Richardson D. S. and Buizza R., *Q. J. R. Meteorol. Soc.*, **125** (1999) 2487-2515.
[47] Houtekamer P. L., Lefaivre L., Derome J., Ritchie H. and Mitchell H., *Mon. Wea. Rev.*, **124** (1996) 1225-1242.
[48] Houtekamer P. L. and Mitchell H., *Mon. Wea. Rev.*, **126** (1998) 796-811.

[49] Jacob C., *The impact of the new cloud scheme on ECMWF's Integrated Forecasting System (IFS)*, in *Proceedings of the ECMWF/GEWEX Workshop on Modeling, Validation and Assimilation of Clouds* (ECMWF, Shinfield Park, Reading RG2 9AX) 1994.
[50] Joly A., Jorgensen D., Shapiro M. A., Thorpe A. J., Bessemoulin P., Browning K. A., Cammas J.-P., Chalon J.-P., Clough S. A., Emanuel K. A., Eymard R., Gall R., Hildebrand P. H., Langland R. H., Lamaître Y., Lynch P., Moore J. A., Persson P. O. G., Snyder C. and Wakimoto R. M., *The Fronts and Atlantic Storm-Track Experiment (FASTEX): Scientific objectives and experimental design*. Report No. 6. The FASTEX Project Office, Météo-France, CNRM, 42 Avenue Coriolis, Toulouse, France. (Also submitted to *Bull. Am. Met. Soc.*) 1996.
[51] Katz R. W., Murphy A. H. and Winkler R. L., *J. Appl. Meteorol.*, **21** (1982) 518-531.
[52] Kontarev G., *The adjoint equation technique applied to meteorological problems*. Technical Report No. 21 (European Centre for Medium-Range Weather Forecasts, Shinfield Park, Reading RG2 9AX, UK) 1980.
[53] Lacarra J.-F. and Talagrand O., *Tellus*, **40A** (1988) 81-95.
[54] Langland R. H. and Rohaly G. D., *Adjoint-based targeting of observations for FASTEX cyclones*, in American Meteorological Society preprints of the *7th Conference on Mesoscale Processes, September 9-13, 1996, Reading, UK* (1996).
[55] Langland R. H., Toth Z., Gelaro R., Szunyogh I., Shapiro M. A., Majumdar S. J., Morss R. E., Rohaly G. D., Velden C., Bond N. and Bishop C. H., *Bull. Amer. Meteor. Soc.*, **80** (1999) 1363-1384.
[56] Le Dimet F.-X. and Talagrand O., *Tellus*, **38A** (1986) 97-110.
[57] Leith C. E., *Mon. Wea. Rev.*, **102** (1974) 409-418.
[58] Lorenz E. N., *J. Atmos. Sci.*, **20** (1963) 130-141.
[59] Lorenz E. N., *Tellus*, **17** (1965) 321-333.
[60] Lorenz E. N., *The Essence of Chaos* (UCL Press) 1993, p. 227.
[61] Mahfouf J.-F., *Tellus*, **51A** (1999) 147-166.
[62] Majumdar S. J., Bishop C. H., Buizza R. and Gelaro R., submitted to *Q. J. R. Meteorol. Soc.*, 2001.
[63] Marsigli C., Montani A., Nerozzi F., Paccagnella T., Tibaldi S., Molteni F. and Buizza R., *A strategy for high resolution ensemble prediction. Part II: limited-area experiments in four Alpine flood events*, to be published in *Q. J. R. Meteorol. Soc.*, 2001.
[64] Mocrette J.-J., *Mon. Wea. Rev.*, **118** (1990) 847-873.
[65] Molteni F. and Palmer T. N., *Q. J. R. Meteorol. Soc.*, **119** (1993) 1088-1097.
[66] Molteni F. and Buizza R., *Mon. Wea. Rev.*, **127** (1999) 2346-2358.
[67] Molteni F., Buizza R., Palmer T. N. and Petroliagis T., *Q. J. R. Meteorol. Soc.*, **122** (1996) 73-119.
[68] Molteni F., Buizza R., Marsigli C., Montani A., Nerozzi F. and Paccagnella T., to be published *Q. J. R. Meteorol. Soc.*, 2001.
[69] Montani A., Thorpe A. J., Buizza R. and Unden P., *Q. J. R. Meteorol. Soc.*, **125** (1999) 3219-3240.
[70] Mullen S. and Buizza R., to be published in *Mon. Wea. Rev.*, 2001.
[71] Noble B. and Daniel J. W., *Applied Linear Algebra* (Prenctice-Hall, Inc.) 1977, p. 477.
[72] Palmer T. N., *On parametrizing scales that are only somewhat smaller than the smallest resolved scales, with application to convection and orography*, in *Proceedings of the ECMWF Workshop on New Insights and Approaches to Convective Parametrization* (ECMWF, Shinfield Park, Reading RG2-9AX, UK) 1997, pp. 328-337.
[73] Palmer T. N., Molteni F., Mureau R., Buizza R., Chapelet P. and Tribbia J., *Ensemble prediction*, in *Proceedings of the ECMWF Seminar on Validation of Models over Europe*, Vol. **I** (ECMWF, Shinfield Park, Reading, RG2 9AX, UK) 1993.
[74] Pu Z.-X., Kalnay E., Sela J. and Szunyogh, *Mon. Wea. Rev.*, **125** (1997) 2479-2503.
[75] Pu Z.-X., Kalnay E. and Toth Z., *Application of the quasi-inverse linear and adjoint NCEP global models to targeted observations during FASTEX*. Preprints of the *12th Conference on Numerical Weather Prediction, 11-16 January 1998, Phoenix, AZ*, (AMS) 1998, p. 8-9.

[76] Puri K., Barkmeijer J. and Palmer T. N., *Q. J. R. Meteorol. Soc.*, **127** (2001) 709-731.
[77] Rabier F., Klinker E., Courtier P. and Hollingsworth A., *Q. J. R. Meteorol. Soc.*, **122** (1996) 121-150.
[78] Richardson L. F., *Weather Prediction by Numerical Process* (Cambridge University Press) (reprint Dover, New York) 1922.
[79] Richardson D. S., *The relative effect of model and analysis differences on ECMWF and UKMO operational forecasts*, in *Proceedings of the ECMWF Workshop on Predictability* (ECMWF, Shinfield Park, Reading RG2 9AX, UK) 1998.
[80] Richardson D. S., *Q. J. R. Meteorol. Soc.*, **126** (2000) 649-668.
[81] Simmons A. J., Burridge D. M., Jarraud M., Girard C. and Wergen W., *Meteorol. Atmos. Phys.*, **40** (1989) 28-60.
[82] Simmons A. J., Mureau R. and Petroliagis T., *Q. J. R. Meteorol. Soc.*, **121** (1995) 1739-1771.
[83] Snyder C., *Bull. Am. Meteor. Soc.*, **77** (1996) 953-961.
[84] Somerville R. C. J., *Predictability and prediction of ultra-long planetary waves* Preprints of the *American Meteoreological Society Fourth Conference on Numerical Weather Prediction* (Silver Spring, MD) (AMS) 1979, pp. 182-185.
[85] Strang G., *Introduction to Applied Mathematics* (Wellesley-Cambridge Press) 1986.
[86] Talagrand O. and Courtier P., *Q. J. R. Meteorol. Soc.*, **113** (1987) 1311-1328.
[87] Talagrand O., Vautard R. and Strauss B., *Evaluation of probabilistic prediction systems*, in *Proceedings of the ECMWF Workshop on Predicability, 20-22 October 1997* (ECMWF, Shienfild Park, Reading RG2-9AX) 1999, pp. 1-26.
[88] Taylor J. and Buizza R., *Energy demand prediction using the ECMWF ensemble prediction system*, to be published in *Int. J. Forecasting* (2001). Also available as ECMWF technical memorandum n. 312, (ECMWF, Shinfield Park, Reading, RG2-9AX, U.K.).
[89] Thorpe A. J. and Shapiro M. A., *FASTEX: Fronts and Atlantic Storm Track Experiment. The Science Plan.* Available form the FASTEX Project Office, July 1995.
[90] Thorpe A. J., Buizza, R., Montani, A. and Palmer T. N., *Chaotic control for weather prediction*, in *Royal Society New Frontiers in Science Exhibition, June 1998* (The Royal Society, 6 Carlton House Terrace, London SW1Y-5AG, UK) 1998.
[91] Tiedtke M., *Mon. Wea. Rev.*, **121** (1993) 3040-3060.
[92] Toth Z. and Kalnay E., *Bull. Am. Met. Soc.*, **74** (1993) 2317-2330.
[93] Tracton M. S. and Kalnay E., *Weather and Forecasting*, **8** (1993) 379-398.
[94] Urban B., *Error maximum growth in simple meteorological models* (in French). Meteorologie Nationale Internal Report, 1985.
[95] Viterbo P. and Beljaars C. M., *J. Clim.*, **8** (1995) 2716-2748.
[96] von Neumann J. and Richtmeyer R. D., *J. Appl. Phys.*, **21** (1950) 232.
[97] Wilks D. S., *Statistical Methods in Atmospheric Sciences* (Academic Press) 1995, (ISBN 0-12-751965-3).
[98] Wilks D. S. and Hamill T. M., *Mon. Wea. Rev.*, **123** (1995) 3564-3575.